nanomaterials

MDPI

Article

Contact Resistance and Channel Conductance of Graphene Field-Effect Transistors under Low-Energy Electron Irradiation

Filippo Giubileo [1,*], Antonio Di Bartolomeo [1,2], Nadia Martucciello [1], Francesco Romeo [1,2], Laura Iemmo [2], Paola Romano [1,3] and Maurizio Passacantando [4]

1. CNR-SPIN Salerno, via Giovanni Paolo II, 132, 84084 Fisciano, Italy; nadia.martucciello@spin.cnr.it
2. Dipartimento di Fisica, Università di Salerno, via Giovanni Paolo II, 132, 84084 Fisciano, Italy; dibant@sa.infn.it (A.D.B.); fromeo@sa.infn.it (F.R.); liemmo@unisa.it (L.I.)
3. Dipartimento di Scienze e Tecnologie, Università del Sannio, via Port'Arsa 11, 82100 Benevento, Italy; promano@unisannio.it
4. Dipartimento di Scienze Fisiche e Chimiche, Università dell'Aquila, Via Vetoio, 67100 L'Aquila, Italy; maurizio.passacantando@aquila.infn.it

* Correspondence: filippo.giubileo@spin.cnr.it; Tel.: +39-89-969329; Fax: +39-89-968817

Academic Editor: Thomas Nann
Received: 22 September 2016; Accepted: 7 November 2016; Published: 10 November 2016

Abstract: We studied the effects of low-energy electron beam irradiation up to 10 keV on graphene-based field effect transistors. We fabricated metallic bilayer electrodes to contact mono- and bi-layer graphene flakes on SiO_2, obtaining specific contact resistivity $\rho_c \approx 19$ kΩ·μm^2 and carrier mobility as high as 4000 cm^2·V^{-1}·s^{-1}. By using a highly doped p-Si/SiO_2 substrate as the back gate, we analyzed the transport properties of the device and the dependence on the pressure and on the electron bombardment. We demonstrate herein that low energy irradiation is detrimental to the transistor current capability, resulting in an increase in contact resistance and a reduction in carrier mobility, even at electron doses as low as 30 e$^-$/nm^2. We also show that irradiated devices recover their pristine state after few repeated electrical measurements.

Keywords: graphene; field-effect transistor; electron irradiation; contact resistance

1. Introduction

Graphene is a promising candidate for future nanoelectronics and has been attracting an enormous amount of attention from the scientific community since 2004, when graphene flakes were exfoliated from graphite for the first time in Manchester [1]. Due to physical limits of Si-technology downscaling, the carbon-based electronics is considered a possible option [2] towards the post-silicon era. Carbon nanotubes (CNTs) have been largely studied in the last two decades but two principal drawbacks have limited their applicability: uncontrollable chirality causing both metallic and semiconducting nanotubes in fabrication processes and the difficulty of correctly placing a large number of nanotubes in integrated circuits. Graphene has reignited the idea of carbon-based electronics, offering unmatched properties such as a linear dispersion relation, with electrons behaving as massless Dirac fermions [3], a very high carrier mobility [4], and a superior current density capability [5]. Graphene is already a reality in applications such as gas sensors [6], photodetectors [7], solar cells [8], heterojunctions [9], and field-effect transistors [10,11].

From an experimental viewpoint, the use of scanning electron microscopy (SEM), transmission electron microscopy (TEM), electron beam lithography (EBL), and focus ion beam (FIB) processing in an ultra-high vacuum represents a necessary step for the fabrication and characterization of graphene-based devices. Consequently, graphene devices during fabrication or under test are

necessarily exposed to a high vacuum and electron irradiation, which may considerably affect their electronic properties.

Several experiments have shown that the irradiation of energetic particles, such as electrons [12–16] and ions [17,18], can induce defects and damages in graphene and cause a severe modifications of its properties.

Raman spectroscopy has been largely used to study electron-beam induced structural modifications [19–21], or formation of nanocrystalline and amorphous carbon [18,22], and to correlate the reduction in 1/f noise in graphene devices with an increasing concentration of defects [23]. The shape and relative magnitude of a D peak, as well as the shift of the G peak, have been used to quantitatively evaluate the damage and the strain induced by a very low energy e-beam [24]. Raman and Auger electron spectroscopy have shown that e-beam irradiation can selectively remove graphene layers and induce chemical reactions and structural transformations [20,21]. The interaction of an e-beam with water adsorbates on the graphene surface has been also proposed for the hydrogenation of graphene [25,26]. However, Raman spectroscopy is unable to reveal all the effects of e-beam irradiation, and electrical measurements are needed to check for possible modifications of transport properties. Despite that, electronic transport properties of irradiated graphene devices have not yet been deeply investigated [27,28]. The negative shift of the Dirac point has been reported as an effect of e-beam-induced n-doping. The comparison with the case of suspended graphene has also evidenced the importance of the substrate [27]: It has been demonstrated in particular that e-beam irradiation of graphene field effect transistors (GFETs) modifies the substrate band bending and results in localized n-doping of graphene, which creates graphene p–n junctions working as a photovoltaic device [29].

In this paper, we study the modification of electronic transport properties of GFETs upon exposure to electron beam irradiation for scanning electron microscopy imaging with an acceleration energy up to 10 keV. An optimized fabrication process has been developed to obtain devices characterized by specific contact resistivity $\rho_c \approx 19\ \mathrm{k\Omega{\cdot}\mu m^2}$ and a carrier mobility as high as 4000 $\mathrm{cm^2{\cdot}V^{-1}{\cdot}s^{-1}}$ on a Si/SiO_2 substrate. Electron irradiation affects the transistor current drive capability by reducing the carrier mobility and increasing the channel and contact resistance. We also show that, for low energy electron irradiation, the conditions of pristine devices are almost restored by successive gate voltage sweeps.

2. Materials and Methods

Graphene flakes were obtained from highly oriented pyrolytic graphite (from NGS Naturgraphit GmbH) by a scotch tape method and were placed on standard p-Si/SiO_2 (300-nm-thick) substrates. After optical identification, the mono- or bi-layer nature of the flakes were confirmed by Raman spectroscopy. Metal contacts to selected graphene flakes were realized by means of electron beam lithography and magnetron sputtering techniques. Spin coating of approximately 400 nm PMMA-A7 (poly-methyl methacrylate) at 4000 rpm was performed on the sample, and it was successively exposed by an EBL system, Raith Elphy Plus (Dortmund, Germany). Methyl isobutyl ketone and then isopropanol was used as a developer. The metal electrodes were fabricated by a three cathode RF Sputtering Magnetron (by MRC Inc., Orangeburg, NY, USA) for in-situ multilayer deposition working at 10^{-7} mbar base pressure. The graphene flakes were contacted by a Nb/Au metallic bilayer (15 nm Nb/25 nm Au) with niobium contacting the graphene and gold working as a cap layer to prevent Nb oxidation and favor electrical connection with the probe tips. Metallic leads were sputtered at low power density (<0.7 $\mathrm{W{\cdot}cm^{-2}}$) and small deposition rates (0.3 nm/s for Nb and 1.2 nm/s for Au) to prevent graphene damages.

Electrical characterization was performed by means of a Janis Research ST-500 cryogenic probe station (Woburn, MA, USA) connected to a Keithley 4200 (Beaverton, OR, USA) Semiconductor Characterization System (SCS) working in wide ranges of current (100 fA to 0.1 A) and voltage (10 μV to 200 V). To study the effect of e-beam irradiation on transistors, the SCS was connected to

a scanning electron microscope Zeiss LEO 1430 (Oberkochen, Germany) equipped with Kleindeik nanomanipulators MM3A (Reutlingen, Germany), which allowed in-situ electrical measurements with the sample inside the high-vacuum SEM chamber to prevent adsorbate contamination.

3. Results and Discussion

3.1. Contact Resistance

In order to characterize the contact resistance, we designed a device with standard geometry to apply the transfer length method (TLM), a structure consisting of a series of spaced electrodes up to 10 μm apart (Figure 1a).

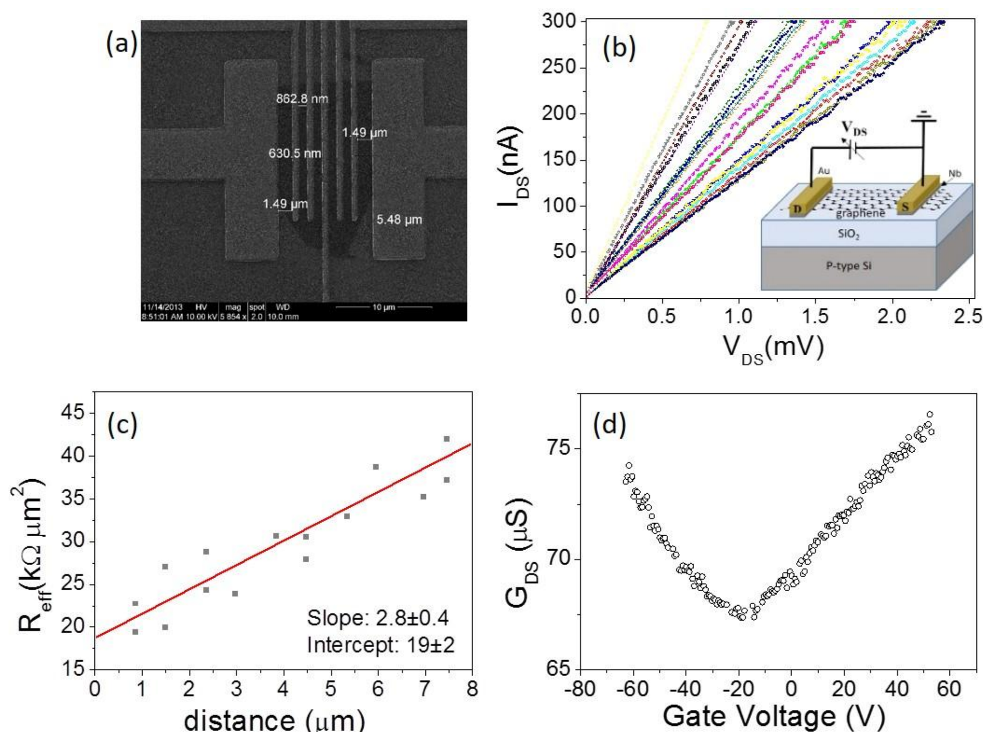

Figure 1. (**a**) A transfer length method (TLM) device with Nb(15 nm)/Au(25 nm) contacts. (**b**) Current–voltage characteristics measured for all possible two-lead combinations in the TLM device, at $V_{\text{Gate}} = 0$ V; inset: scheme of the device. (**c**) TLM plot of R_{eff} (L) at $V_{\text{Gate}} = 0$ V. (**d**) Transfer characteristic of one of the back-gated transistors of (a) in the range -60 V < V_{Gate} < +60 V.

The two-probe current–voltage characteristic of the channel (I_{DS} vs. V_{DS}) has been measured for each possible combination of contacts: the drain current (I_{DS}) linearly increases with source-drain voltage (V_{DS}), which is a typical behavior at low bias (Figure 1b). According to the TLM, we can extract the specific contact resistivity ρ_c by evaluating (for the general situation of irregular shaped flakes) the intercept of a plot of R_{eff} vs. L [30], with L the separation between the two electrodes, and

$$R_{\text{eff}} = R\left(\frac{1}{W_1 d_1} + \frac{1}{W_2 d_2}\right)^{-1}$$

where W_i and d_i (for $i = 1, 2$) indicate width and length of each contact, respectively. From the linear fitting of R_{eff} vs. L (see Figure 1c), we find $\rho_c = 19 \pm 2$ kΩ·μm^2, an intermediate value compared with previously reported values of 7 kΩ·μm^2 for Ni and 30 kΩ·μm^2 for Ti [31].

We also tested the current modulation of this device when used as a field effect transistor with the Si substrate as the back-gate electrode. In Figure 1d, we report the transfer characteristic G_{DS}

vs. V_{Gate} in which the channel conductance G_{DS} is measured as a function of the gate voltage V_{Gate} between a couple of electrodes biased at V_{DS} = 0.5 mV. The conductance clearly shows a minimum at $V_{Gate} = -15$ V, corresponding to the charge neutrality point (Dirac point). The negative value indicates that the graphene is *n*-doped. The device was measured as produced, without any electrical annealing (stress), which is suitable for inducing the desorption of surface contaminants and improving the metal-graphene coupling, thus reducing the contact resistance [5]. In Figure 2, we show the output characteristics (I_{DS} vs. V_{DS} for several V_{Gate} values in the range -60 V to +60 V) and the transfer characteristic (at fixed V_{DS}) measured before and after an electrical stress event that stabilize the device improving its performances. The black arrow in the figure identifies the voltage at which the device was suddenly modified, switching from a total resistance of about 250 kΩ to 150 kΩ, for the effect of current annealing. After such modification, the device was routinely measured, showing extreme stability without further modification of the total resistance R_{DS}, which we report as a function of V_{Gate} in the insets of Figure 2. R_{DS} is the series of the contact resistance and the channel resistance, $R_{DS} = R_C + R_{channel}$, where the channel resistance can be expressed as $R_{channel} = \frac{L/W}{\mu\ n(V_{bg})\ q}$ with L and W the length and width of the channel, respectively, μ is the carrier mobility, and q is the unit charge [32]. The total carrier concentration can be written $\left(V_{bg}^*\right) = \sqrt{n_{ind}^2 + n_0^2}$, where V_{bg}^* is the back-gate voltage with respect to the Dirac voltage ($V_{bg}^* = V_{bg} - V_{Dirac}$), n_0 is the intrinsic carrier concentration, and n_{ind} is the carrier concentration induced by the back gate. n_{ind} can be expressed in terms of gate oxide capacitance as $n_{ind}\left(V_{bg}^*\right) = C_{ox}V_{bg}^*/q$. This model, adapted to the experimental data R vs. V_{Gate} allows for the extraction of the contact resistance and carrier mobility as fitting parameters.

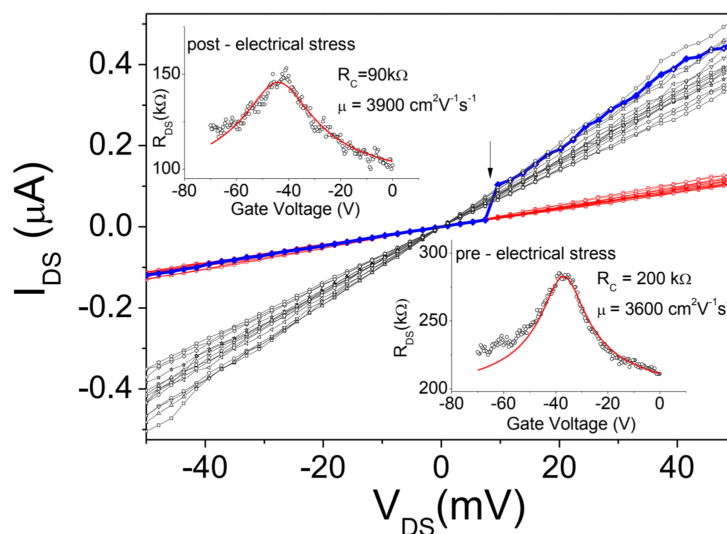

Figure 2. Output characteristics (I_{DS} vs. V_{DS}) and transfer characteristics (R_{DS} vs. V_{Gate} in the insets) measured before and after the stabilization of the device due to electrical stress. Black arrow indicates the switch from higher to lower total resistance. Continuous (red) lines in the insets represent the numerical simulations obtained from the model of [32]. The contact resistance $R_{contact}$ is abbreviated as R_C in the figures.

Using the transfer characteristics measured before and after the electrical stress, we found that the contact resistance improved (reduced from 200 kΩ to 90 kΩ), while the carrier mobility increased from 3600 $V^2 \cdot cm^{-1} \cdot s^{-1}$ to 3900 $V^2 \cdot cm^{-1} \cdot s^{-1}$. The electrical stress increased the graphene–metal coupling and worked to clean the channel. The mobility values are comparable to values already reported for Nb-contacted GFETs [33]. We also noticed that the characteristic measured before the electrical stress showed an asymmetric shape, with the *p*-branch clearly away from the expected theoretical behavior. This can be explained in terms of the reduced coupling between the Nb electrode and the graphene

channel (corresponding to large contact resistance), a situation that can cause asymmetry, a double dip, or both in such curves as reported in [33,34]. The improvement of the contact after electrical stress, resulting in better coupling between Nb and graphene, removed the asymmetry. Comparing the channel resistances that were extracted as $R_{DS} - R_{contact}$ we also confirmed the improvement of the channel resistance.

In Figure 3, we show the electrical characterization of two other representative devices of the dozen produced in the same batch, after stabilization by electrical stress. The curves of Figure 3a,b are the output characteristics measured in a high vacuum (10^{-7} mbar) for different gate voltage values. The ohmic nature of the contacts is confirmed by the linearity of such characteristics.

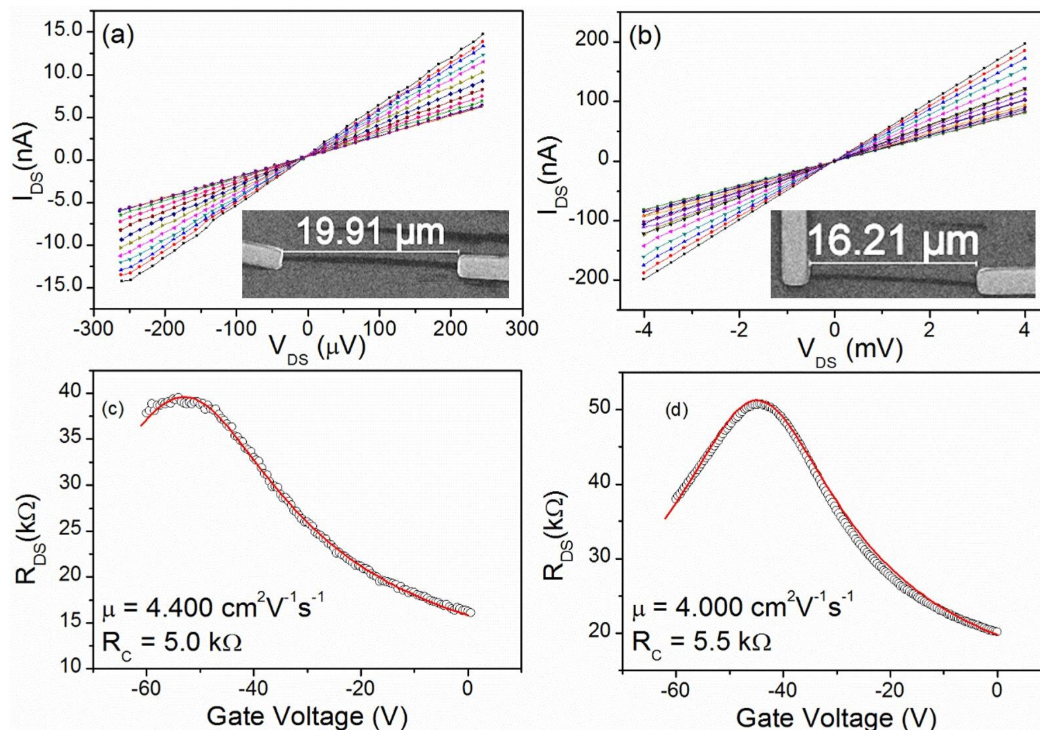

Figure 3. Electrical characterization under a high vacuum of two devices produced on the same substrate. (**a**,**b**) I_{DS} vs. V_{DS} curves for the devices shown in the insets with dimensions 19.9 μm × 0.7 μm and 16.2 μm × 0.3 μm, respectively. Curves are measured for different gate voltages in the range -60 V < V_{Gate} < 0 V with steps of 5 V. (**c**,**d**) R_{DS} vs. V_{Gate} curves measured at V_{DS} = 1 mV for the devices of Figure 3a,b, respectively. The solid (red) lines are the fitted model of [32] with the parameters listed in the plots.

In Figure 3c,d, we show the corresponding transfer characteristics measured at fixed drain-source bias V_{DS} = 1 mV. Remarkably, the current annealing and the long high vacuum storage produced very stable devices with low contact resistance (5.0 kΩ < $R_{contact}$ < 5.5 kΩ). The high fabrication quality is confirmed by the small contact resistance, the low noise, and the high carrier mobility, which is 4000 $V^2 \cdot cm^{-1} \cdot s^{-1}$ < μ < 4400 $V^2 \cdot cm^{-1} \cdot s^{-1}$. The Dirac point at a bias between -40 V and -60 V indicates a strong *n*-doping that is favored by the vacuum and the electron irradiation (this measurements was performed inside a SEM, post imaging).

As soon as the devices are exposed to air, the graphene collects adsorbates that, generally acting as *p*-dopants, shift the Dirac point towards positive biases, increase the contact resistance and reduce the carrier mobility [6,35–39]. Figure 4 compares the transfer characteristics of the device of Figure 3c measured in a high vacuum and soon after exposure to air. From the fit of the model, we extracted the contact resistance in air, as $R_{contact} \approx 6.7$ kΩ a value 35% larger than the value in the high vacuum, while the carrier mobility was reduced to μ ≈ 4100 $V^2 \cdot cm^{-1} \cdot s^{-1}$. The inset shows the evolution of the

Dirac point from −55 V in the high vacuum to −30 V in air. This observation confirms the importance of performing the electrical measurements in-situ when studying irradiation effects to distinguish the electron beam from other environment-induced phenomena.

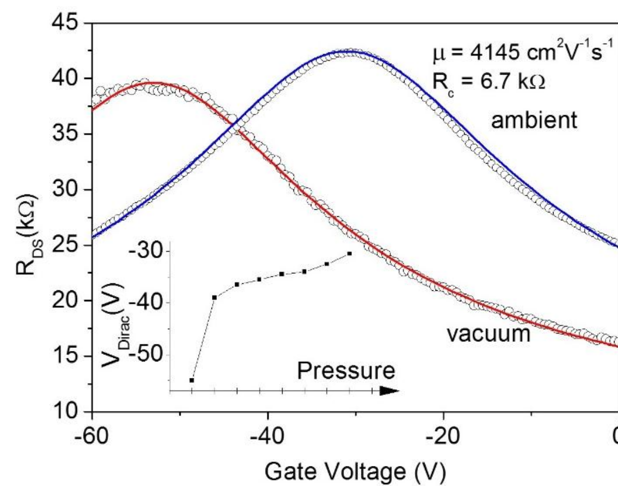

Figure 4. The effect of the pressure variation from high vacuum to ambient conditions on the R_{DS} vs. V_{Gate} curve reported in Figure 3a. Solid lines are the fitting curves. Inset: evolution of the Dirac point for increasing pressure.

3.2. *Effect of Electron Beam Irradiation*

In the following, we consider the effect of electron beam irradiation on the GFETs. In particular, we consider electron beam energy up to 10 keV, i.e., the energy range typically used for SEM imaging. Larger energy (about 30 keV) is normally used for e-beam lithography or imaging in STEM mode. The irradiation was performed on an area of 20 μm × 20 μm, covering most of the graphene channel, with constant beam current I_{beam} = 0.2 nA. We used an exposure time of 10 s, which resulted in an electron irradiation dose of about 30 e^-/nm^2. Differently from other works [27], we performed post-irradiation electrical measurements directly in the SEM chamber, thus avoiding the aforementioned effects of air. Results obtained in six successive electrical sweeps, after a 10 s electron irradiation at 10 keV, are reported in Figure 5a. The complete (forward and backward) sweeping between 0 V and −70 V evidences an important hysteresis that decreases with successive electrical sweeps. The appearance of the hysteresis is easily explained by mobile electrons that are trapped in the gate oxide during e-beam exposure and that screen the gate voltage, while the hysteresis reduction can be caused by their withdrawal by the channel during the successive voltage sweeps [40,41]. By comparing the transfer characteristic before the electron irradiation to the first and sixth sweep measured after the 10 s exposure (Figure 5b), we observe that the device initially has a significant variation in the channel conductance, with considerably reduced gate modulation and reduced carrier mobility, while after successive sweeps it returned to its initial state apart a marginal shift of the Dirac point. To quantitatively analyze the evolution after e-beam exposure (see Figure 5c), we used the model of [32] to estimate the transport parameters, which are summarized in Figure 5d. The carrier mobility is reduced by the 10 s e-beam irradiation from 4000 $V^2 \cdot cm^{-1} \cdot s^{-1}$ to about 3600 $V^2 \cdot cm^{-1} \cdot s^{-1}$ (as obtained from the first sweep measurement). The initial value is restored by the successive sweeps. A consistent behavior is shown by the total resistance, which is increased by the irradiation and recovers with an increasing number of sweeps. The increase in total resistance, as a consequence of the e-beam irradiation, has also been observed on chemical vapor deposition (CVD) grown graphene [42]. Figure 5d reports the effect of irradiation on the contact resistance that is increased by about 70% by the exposure and is smoothly restored by successive sweeps. Noticeably, the irradiation seems to have a negligible effect on the intrinsic carrier concentration n_0. Mobility and resistance degradation can

be explained as increased long-range coulomb scattering [43] by electrons stored in the gate oxide during e-beam exposure (damaging of graphene seems to have a minor contribution); such electrons are gradually removed by voltage application during successive sweeps, and pristine conditions are partially recovered.

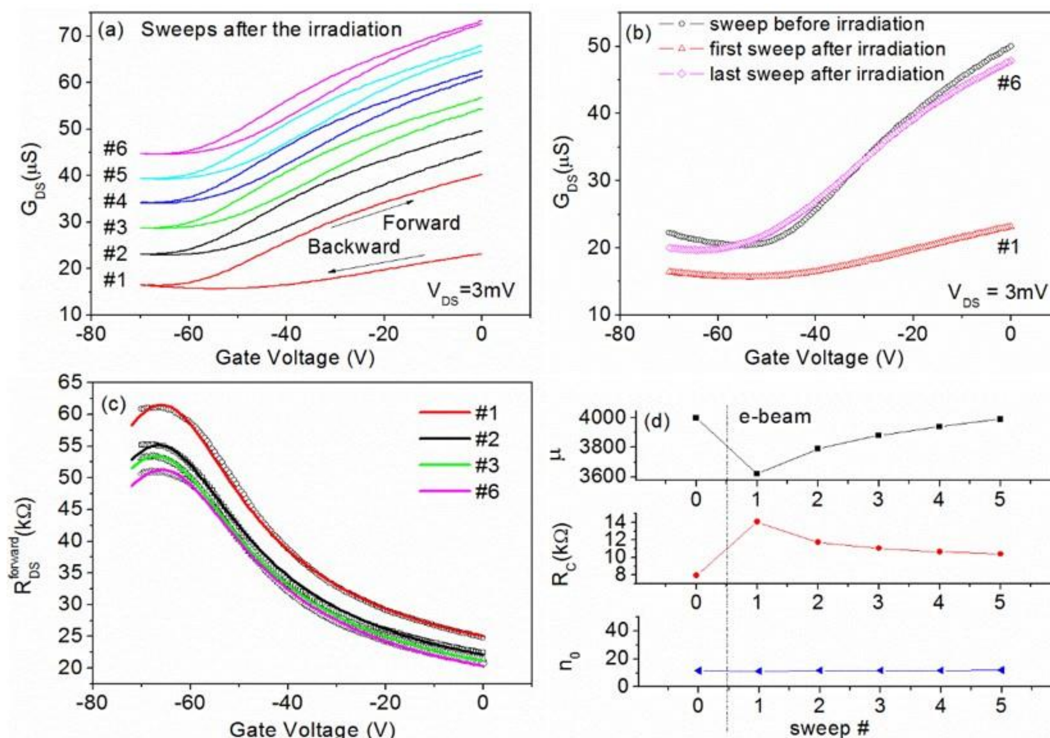

Figure 5. Effect of electron irradiation on R_{DS} vs. V_{Gate} of graphene field effect transistors (GFETs) characterized in Figure 3c. (**a**) Six successive sweeps recorded soon after the electron irradiation. Curves have been shifted for clarity. (**b**) Comparison of the first and sixth sweep after the 10 s e-beam exposure with that measured on unexposed device. (**c**) Forward sweep of selected measurements and relative fitting curves according to the model [32]. (**d**) Summary of parameters extracted by fitting of the curves corresponding to forward sweeps.

4. Conclusions

We realized graphene-based field effect transistors on a Si/SiO_2 substrate with Nb/Au metallic bilayers as contacting electrodes. Electrical characterization evidenced high-quality devices with carrier mobility as high as 4000 $cm^2 \cdot V^{-1} \cdot s^{-1}$ and specific contact resistivity of about 19 kΩ·µm^2. The effect of 10 keV electron irradiation, with a dose of 30 e^-/nm^2, on the transport properties has been reported, evidencing a significant reduction in carrier mobility and an increase in contact resistance. Finally, we show here that, for low energy irradiation, the pristine conditions are almost restored after several electrical sweeps, which we explain as a gradual removal of electrons piled up in the gate oxide during e-beam exposure.

Acknowledgments: All sources of funding of the study should be disclosed. Please clearly indicate grants that you have received in support of your research work. Clearly state if you received funds for covering the costs to publish in open access.

Author Contributions: Filippo Giubileo, Antonio Di Bartolomeo and Maurizio Passacantando conceived and designed the experiments; Filippo Giubileo, Francesco Romeo and Maurizio Passacantando performed the experiments; Filippo Giubileo, Antonio Di Bartolomeo, Francesco Romeo, Laura Iemmo, Nadia Martucciello and Paola Romano analyzed the data; Filippo Giubileo and Antonio Di Bartolomeo wrote the paper.

Conflicts of Interest: The authors declare no conflict of interest.

References

1. Novoselov, K.S.; Geim, A.K.; Morozov, S.V.; Jiang, D.; Zhang, Y.; Dubonos, S.V.; Grigorieva, I.V.; Firsov, A.A. Electric field effect in atomically thin carbon films. *Science* **2004**, *306*, 666–669. [CrossRef] [PubMed]
2. Chau, R.; Datta, S.; Doczy, M.; Doyle, B.; Jin, B.; Kavalieros, J. Benchmarking Nanotechnology for High-Performance and Low-Power Logic Transistor Applications. *IEEE Trans Nanotechnol.* **2005**, *4*, 153–158. [CrossRef]
3. Castro Neto, A.H.; Guinea, F.; Peres, N.M.R.; Novoselov, K.S.; Geim, A.K. The electronic properties of graphene. *Rev. Mod. Phys.* **2009**, *81*, 109–162. [CrossRef]
4. Du, X.; Skachko, I.; Barker, A.; Andrei, E.Y. Approaching ballistic transport in suspended graphene. *Nat. Nanotechnol.* **2008**, *3*, 491–495. [CrossRef] [PubMed]
5. Moser, J.; Barreiro, A.; Bachtold, A. Current-induced cleaning of graphene. *Appl. Phys. Lett.* **2007**, *91*, 163513. [CrossRef]
6. Schedin, F.; Geim, A.K.; Morozov, S.V.; Hill, E.V.; Blake, P.; Katsnelson, M.I.; Novoselov, K.S. Detection of individual gas molecules adsorbed on graphene. *Nat. Mater.* **2007**, *6*, 652–655. [CrossRef] [PubMed]
7. Xia, F.; Mueller, T.; Lin, Y.M.; Valdes-Garcia, A.; Avouris, P. Ultrafast graphene photodetector. *Nat. Nanotechnol.* **2009**, *4*, 839–843. [CrossRef] [PubMed]
8. Li, X.M.; Zhu, H.W.; Wang, K.L.; Cao, A.Y.; Wei, J.Q.; Li, C.Y.; Jia, Y.; Li, Z.; Li, X.; Wu, D.H. Graphene-on-Silicon Schottky Junction Solar Cells. *Adv. Mater.* **2010**, *22*, 2743–2748. [CrossRef] [PubMed]
9. Di Bartolomeo, A. Graphene Schottky diodes: An experimental review of the rectifying graphene/semiconductor heterojunction. *Phys. Rep.* **2016**, *606*, 1–58. [CrossRef]
10. Schwierz, F. Graphene transistors. *Nat. Nanotechnol.* **2010**, *5*, 487–496. [CrossRef] [PubMed]
11. Di Bartolomeo, A.; Giubileo, F.; Iemmo, L.; Romeo, F.; Russo, S.; Unal, S.; Passacantando, M.; Grossi, V.; Cucolo, A.M. Leakage and field emission in side-gate graphene field effect transistors. *Appl. Phys. Lett.* **2016**, *109*, 023510. [CrossRef]
12. Buchowicz, G.; Stone, P.R.; Robinson, J.T.; Cress, C.D.; Beeman, J.W.; Dubon, O.D. Correlation between structure and electrical transport in ion-irradiated graphene grown on Cu foils. *Appl. Phys. Lett.* **2011**, *98*, 032102. [CrossRef]
13. Kalbac, M.; Lehtinen, O.; Krasheninnikov, A.V.; Keinonen, J. Ion-Irradiation-Induced Defects in Isotopically-Labeled Two Layered Graphene: Enhanced In-Situ Annealing of the Damage. *Adv. Mater.* **2013**, *25*, 1004–1009. [CrossRef] [PubMed]
14. Chen, J.H.; Cullen, W.G.; Jang, C.; Fuhrer, M.S.; Williams, E.D. Defect Scattering in Graphene. *Phys. Rev. Lett.* **2009**, *102*, 236805. [CrossRef] [PubMed]
15. Compagnini, G.; Giannazzo, F.; Sonde, S.; Raineri, V.; Rimini, E. Ion irradiation and defect formation in single layer graphene. *Carbon* **2009**, *47*, 3201–3207. [CrossRef]
16. Guo, B.; Liu, Q.; Chen, E.; Zhu, H.; Fang, L.; Gong, J.R. Controllable N-Doping of Graphene. *Nano Lett.* **2010**, *10*, 4975–4980. [CrossRef] [PubMed]
17. Kotakoski, J.; Krasheninnikov, A.; Kaiser, U.; Meyer, J. From Point Defects in Graphene to Two-Dimensional Amorphous Carbon. *Phys. Rev. Lett.* **2011**, *106*, 105505. [CrossRef] [PubMed]
18. Teweldebrhan, D.; Balandin, A.A. Modification of graphene properties due to electron-beam irradiation. *Appl. Phys. Lett.* **2009**, *95*, 013101. [CrossRef]
19. Krasheninnikov, A.V.; Banhart, F. Engineering of nanostructured carbon materials with electron or ion beams. *Nat. Mater.* **2007**, *6*, 723–733. [CrossRef] [PubMed]
20. Warner, J.H.; Rummeli, M.H.; Ge, L.; Gemming, T.; Montanari, B.; Harrison, N.M.; Buchner, B.; Briggs, G.A. Structural transformations in graphene studied with high spatial and temporal resolution. *Nat. Nanotechnol.* **2009**, *5*, 500–504. [CrossRef] [PubMed]
21. Xu, M.; Fujita, D.; Hanagata, N. Monitoring electron-beam irradiation effects on graphenes by temporal Auger electron spectroscopy. *Nanotechnology* **2010**, *21*, 265705. [CrossRef] [PubMed]
22. Teweldebrhan, D.; Balandin, A.A. Response to "Comment on 'Modification of graphene properties due to electron-beam irradiation'". *Appl. Phys. Lett.* **2009**, *95*, 246102. [CrossRef]
23. Hossain, M.Z.; Rumyantsev, S.; Shur, M.S.; Balandin, A.A. Reduction of 1/f noise in graphene after electron-beam irradiation. *Appl. Phys. Lett.* **2013**, *102*, 153512. [CrossRef]

24. Murakami, K.; Kadowaki, T.; Fujita, J. Damage and strain in single-layer graphene induced by very-low-energy electron-beam irradiation. *Appl. Phys. Lett.* **2013**, *102*, 043111. [CrossRef]
25. Jones, J.D.; Mahajan, K.K.; Williams, W.H.; Ecton, P.A.; Mo, Y.; Perez, J.M. Formation of graphane and partially hydrogenated graphene by electron irradiation of adsorbates on graphene. *Carbon* **2010**, *48*, 2335–2340. [CrossRef]
26. Jones, J.D.; Ecton, P.A.; Mo, Y.; Perez, J.M. Comment on "Modification of graphene properties due to electron-beam irradiation". *Appl. Phys. Lett.* **2009**, *95*, 246101. [CrossRef]
27. Childres, I.; Jauregui, L.A.; Foxe, M.; Tian, J.; Jalilian, R.; Jovanovic, I.; Chen, Y.P. Effect of electron-beam irradiation on graphene field effect devices. *Appl. Phys. Lett.* **2010**, *97*, 173109. [CrossRef]
28. He, Y.H.; Wang, L.; Chen, L.; Wu, Z.F.; Li, W.; Cai, Y.; Wang, N. Modifying electronic transport properties of graphene by electron beam irradiation. *Appl. Phys. Lett.* **2011**, *99*, 033109. [CrossRef]
29. Yu, X.; Shen, Y.; Liu, T.; Wu, T.T.; Wang, Q.J. Photocurrent generation in lateral graphene p-n junction created by electron-beam irradiation. *Sci. Rep.* **2015**, *5*, 12014. [CrossRef] [PubMed]
30. Di Bartolomeo, A.; Santandrea, S.; Giubileo, F.; Romeo, F.; Petrosino, M.; Citro, R.; Barbara, P.; Lupina, G.; Schroeder, T.; Rubino, A. Effect of back-gate on contact resistance and on channel conductance in graphene-based field-effect transistors. *Diam. Relat. Mater.* **2013**, *38*, 19–23. [CrossRef]
31. Di Bartolomeo, A.; Giubileo, F.; Iemmo, L.; Romeo, F.; Santandrea, S.; Gambardella, U. Transfer characteristics and contact resistance in Ni- and Ti-contacted graphene-based field-effect transistors. *J. Phys. Condens. Matter* **2013**, *25*, 155303. [CrossRef] [PubMed]
32. Venugopal, A.; Colombo, L.; Vogel, E.M. Issues with characterizing transport properties of graphene field effect transistors. *Solid State Comm.* **2012**, *152*, 1311–1316. [CrossRef]
33. Di Bartolomeo, A.; Giubileo, F.; Romeo, F.; Sabatino, P.; Carapella, G.; Iemmo, L.; Schroeder, T.; Lupina, G. Graphene field effect transistors with niobium contacts and asymmetric transfer characteristics. *Nanotechnology* **2015**, *26*, 475202. [CrossRef] [PubMed]
34. Di Bartolomeo, A.; Giubileo, F.; Santandrea, S.; Romeo, F.; Citro, R.; Schroeder, T.; Lupina, G. Charge transfer and partial pinning at the contacts as the origin of a double dip in the transfer characteristics of graphene-based field-effect transistors. *Nanotechnology* **2011**, *22*, 275702. [CrossRef] [PubMed]
35. Ryu, S.; Liu, L.; Berciaud, S.; Yu, Y.J.; Liu, H.; Kim, P.; Flynn, G.W.; Brus, L.E. Atmospheric Oxygen Binding and Hole Doping in Deformed Graphene on a SiO_2 Substrate. *Nano Lett.* **2010**, *10*, 4944–4951. [CrossRef] [PubMed]
36. Leenaerts, O.; Partoens, B.; Peeters, F.M. Adsorption of H_2O, NH_3, CO, NO_2, and NO on graphene: A first-principles study. *Phys. Rev. B* **2008**, *77*, 125416. [CrossRef]
37. Pirkle, A.; Chan, J.; Venugopal, A.; Hinojos, D.; Magnuson, C.W.; McDonnell, S.; Colombo, L.; Vogel, E.M.; Ruoff, R.S.; Wallace, R.M. The effect of chemical residues on the physical and electrical properties of chemical vapor deposited graphene transferred to SiO_2. *Appl. Phys. Lett.* **2011**, *99*, 122108. [CrossRef]
38. Suk, J.W.; Lee, W.H.; Lee, J.; Chou, H.; Piner, R.D.; Hao, Y.; Akinwande, D.; Ruoff, R.S. Enhancement of the Electrical Properties of Graphene Grown by Chemical Vapor Deposition via Controlling the Effects of Polymer Residue. *Nano Lett.* **2013**, *13*, 1462–1467. [CrossRef] [PubMed]
39. Ni, Z.H.; Wang, H.M.; Luo, Z.Q.; Wang, Y.Y.; Yu, T.; Wu, Y.H.; Shena, Z.H. The effect of vacuum annealing on graphene. *J. Raman Spectrosc.* **2010**, *41*, 479–483. [CrossRef]
40. Wang, H.; Wu, Y.; Cong, C.; Shang, J.; Yu, T. Hysteresis of Electronic Transport in Graphene Transistors. *ACS Nano* **2010**, *4*, 7221–7228. [CrossRef] [PubMed]
41. Di Bartolomeo, A.; Rinzan, M.; Boyd, A.K.; Yang, Y.; Guadagno, L.; Giubileo, F.; Barbara, P. Electrical properties and memory effects of field-effect transistors from networks of single- and double-walled carbon nanotubes. *Nanotechnology* **2010**, *21*, 115204. [CrossRef] [PubMed]
42. Iqbal, M.Z.; Singh, A.K.; Iqbal, M.W.; Seo, S.; Eom, J. Effect of e-beam irradiation on graphene layer grown by chemical vapor deposition. *J. Appl. Phys.* **2012**, *111*, 084307. [CrossRef]
43. Chen, J.H.; Jang, C.; Adam, S.; Fuhrer, M.S.; Williams, E.D.; Ishigami, M. Charged-impurity scattering in graphene. *Nat. Phys.* **2008**, *4*, 377–381. [CrossRef]

© 2016 by the authors; licensee MDPI, Basel, Switzerland. This article is an open access article distributed under the terms and conditions of the Creative Commons Attribution (CC-BY) license (http://creativecommons.org/licenses/by/4.0/).